Design of a Variable Stiffness Mechanism with Prescribed Behaviour Using a Variable Cam Pulley

Floris van Ruitenbeek, *BSc Student EE, University of Twente*

***Abstract*—Compliant robotics has the potential to further automate the agri-food industry by allowing delicate interaction with products of varying types and sizes. Compliant gripper designs often require non-linear springs to vary compliance/stiffness of the system. Springs with prescribed force-deflection curves are not readily available. This paper presents a variable stiffness mechanism based on a variable radius pulley placed in series with a linear spring. The mechanism is designed for use in a tendon-based gripper prototype of which previous non-linear springs did not perform well. An iterative, feedback-based method for generating a pulley profile following a desired force-deflection curve is constructed. Other symbolic and performance-metric-based approaches are discussed. Mathematical approximations limit the expected accuracy of generated profiles. A proof-of-concept setup is built to test a range of generated profiles. Resulting measurements show strong correlation between desired and measured force-deflection curves. Error, likely resulting from mathematical approximations and material deformation, is mainly present at the higher non-linearity profiles, where the measurements deviate further from the desired values. Further focus on eliminating the mathematical approximations should result in a promising design that is easy to customize, simple to construct, and low friction.**

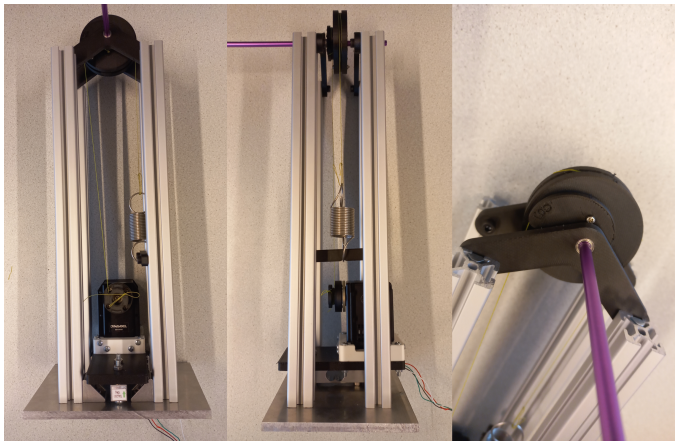

Fig. 1: Several views of the realised non-linear spring test-setup

I. Introduction

THE agri-food industry requires delicate grasping with varying types of products. Challenges arise when factors between products change, like weight, size and compliance. In automation, most robotic grippers are optimized to work with predictable/similar objects, instead of a wide range of varying objects. More automation in this sector requires research towards a new approach; active compliant grippers. Unlike most common grippers, active compliant grippers can vary joint stiffness when required to. Fragile objects can be carefully grasped (high compliance), while grasped objects can resist external forces (low compliance). This extra level of adjustment makes (active) compliant grippers suitable for handling varying and fragile objects.

Many variable stiffness mechanisms have been designed already. R. V. Ham et al. [1] review several active and passive controllable stiffness actuators. Methods like the agonist-antagonist setup require combining series-elastic actuation (SEA) with non-linear elements to vary stiffness. Mechanism-based examples include the basic cam-follower approach by S.A. Migliore et al. [2]. A set of guided "rollers", distanced by a linear spring, move over a contour. By increasing distance between rollers, a specific force-deflection relation is created. The cam-follower method is tunable by altering these cams/contours. In addition to this, several designs are made using a "variable-cam pulley" approach. N. Schmit et al. [3] describe a nonlinear rotational spring, formed by connecting a translational spring to a tendon from a variable-cam pulley. C.B. Yigit et al. [4] show several complex algorithms, analytical and iterative, to create a nonlinear translational spring, using a torsion spring instead. J. Malzahn et al. [5] present a fixed passive rolling flexure design utilizing the change of length of a flexure. Other methods include material or magnetism-based approaches using rubber or magnets to create non-linear elements [6][7][8].

A MSc-thesis paper by M. Bluiminck [9] showcasing a promising prototype which utilizes variable compliance is looked at. The prototype features an 2-DoF tendon-driven finger-based gripper. An agonist-antagonist approach is used to create variable stiffness and position control on the phalanges. This approach requires the use of nonlinear springs (NLS) in the mechanism, to allow for variable stiffness. The design currently utilises the basic cam-follower mechanism mentioned above. This NLS design suffers from deviation between ideal and realistic behaviour, and is large in size. These non-idealities cause deviations between simulated and measured gripper states, lowering gripper performance. Measured force-deflection curves of the current NLS implementation follow the desired spring behaviour closely. However, especially towards higher tensile forces, measurements show stick-slip-like behaviour. Possible causes include high friction, printing defects and binding. More broadly, the high friction nature of the spring mechanism has the potential to cause differences between simulated and realistic gripper states.

This paper focuses on designing an improved NLS mechanism, both to increase performance and reduce size. This design should be customizable to fit a wider range of spring-

deflection curves, such that the approach used can be adopted for other applications requiring NLS's. The presented design uses the previously mentioned variable-cam pulley principle. A tendon connected to a non-circular pulley is deflected, while a torsion spring is placed between the pulley axle and base/ground (see Fig. 2). The pulley and spring together form the nonlinear spring mechanism. When implemented into e.g. the gripper prototype, the torsion spring connects to a servo instead of ground, which enables variable/controllable equilibrium and stiffness of the phalanges in the agonist-antagonist system. The pulley-approach is used due to its mechanically simple nature, little moving parts, and low friction properties. Also presented is a test setup (Fig. 1) used to compare performance of several synthesized spring profiles to their simulated counterparts. Several assumptions are made in the analysis of the system, which should result in deviations from simulated data. The research question for this project is as follows;

"How to design a spring with prescribed non-linear force-deflection to be compact and low friction?"

This paper is organized as follows; Sec. II lists requirements, explains the NLS mechanism in more detail and evaluates several methods to calculate a pulley-cam from a desired force-deflection curve. Sec. III discusses two different NLS implementations, including a realised test-setup and the experiments to be carried out. Sec. IV lists the corresponding results, and Sec. V and VI subsequently provide a discussion and conclusion to the paper.

II. Concept and Analysis

This section lists design requirements, and explains the non-linear spring mechanism in detail. Generating pulley profiles is of key importance to match desired force-deflection behaviour. Thus, several methods toward calculating pulley profiles are evaluated, of which only the third is deemed sufficient and is used for further design.

A. Requirements

The gripper prototype currently uses 2 NLS's with varying strengths ($F_1(x)$ and $F_2(x)$). The force-deflection (F-D) relations of the currently used NLS units are as follows:

$$F_1 = 1.91x^2 - 1.13x + 1.53,\ F_2 = 3.81x^2 - 3.24x + 2.59 \quad (1)$$

where F_i denotes the tensile force induced in the tendon, and x denotes tendon deflection in cm (for better readability further in the paper). Spring 2 should be twice as strong as spring 1, to result in the previously mentioned variable stiffness in the gripper [9]. These curves are used as baseline for the requirements. The gripper prototype requires springs to displace approximately $6.5cm$. The precise shape of the F-D curve does not matter for the prototype, as long as they are scaled with a factor two, equally nonlinear, and have approximately the same force range.

Additionally, the mechanism should be as low-friction as possible, since friction could lead to an increase in system hysteresis. Size restrictions are not clearly stated as future gripper prototypes would likely change. A side view of one of the current mechanisms is approx. $12\text{x}12cm$. A smaller mechanism is desired.

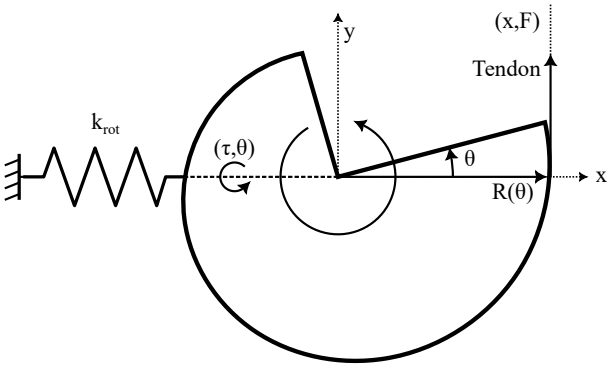

Fig. 2: Schematic of variable stiffness mechanism

B. Mechanism

Placing in series a linear spring and non-linear transmission element, a nonlinear spring mechanism is formed. In this case a linear torsion spring is placed on the axle of a pulley, shown in Fig. 2. This pulley varies its radius, thus force-arm, based on its rotation. This allows the pulley to function as a modulated transformer. A tendon is wound around the pulley profile up along the y-axis. The tensile force experienced in the tendon depends on the force-arm experienced at that instant. Displacing the tendon results in a change of rotation of the pulley, thus changing the force-arm. A decrease in force-arm length results is decreased torque on the axle to the spring. Thus, a nonlinear spring mechanism is formed.

Fig. 2 shows an overview of the system where; (x, F) equals the tendon deflection and tensile force, (θ, τ) the pulley rotation and torque, $R(\theta)$ the pulley radius at deflection angle θ, and k_{rot} the torsion spring constant. To decrease complexity of the mathematics behind the mechanism, some assumptions/approximations are taken. These approximations significantly change the accuracy of the calculations, as we will see later on in Sec. IV. The following list sums up the approximations taken;

- The tangential/detachment point of the tendon is always located on the x-axis and does not shift as a result of variable radius. Thus, $R(\theta)$ directly results in the force-arm experienced by the tendon.
- Tensile force on the tendon always acts at a right angle to the force arm creating torque.
- Tensile force in the tendon acts purely on the tangential/detachment point of the tendon to create torque, and is not distributed over the profile circumference.
- The tendon always leaves the pulley cam perfectly vertical, independent of length between tendon and end-point, and pulley orientation.
- The tendon always "sticks" to the pulley profile, thus any concave shape is not allowed.

The first two approximations listed have the most impact on the measurements. The detachment point of a tendon on

a pulley is always located where the tangent is in-line with the tangent of the pulley surface. On a circular pulley and assuming a vertical tendon, this will always be on the $x\text{-}axis$. However, when the pulley varies its radius, this assumption no longer holds. This means the force arm the pulley experiences is not exactly equal to radius R at a certain pulley angle θ. The actual arm over which torque is produced will lag behind the radius the simulation has generated. In addition, when this tangent is not at a right angle, the force on the pulley will be a smaller component of the tensile force on the tendon. These inaccuracies lead to differences between simulation and measurements. Measured responses are expected to show lower force values than simulations. Sec. IV reflects this behaviour.

Three different approaches to formulate a profile for a certain desired F-D curve are demonstrated. The third method, involving an iterative solution, is most flexible and is used to generate the profiles under Sec. III.

C. Solve Symbolically

Solving the problem symbolically is ideal. This would result in a solution that can easily be used to convert any desired curve to a pulley profile, without complications. Given the previously stated assumptions we can assume that the tensile force on the tendon is given by:

$$F(\theta) = \frac{1}{R(\theta)}\tau \tag{2}$$

Subsequently, the torque created by the spring is given by:

$$\tau = k_{rot}\theta \rightarrow F(\theta) = \frac{1}{R(\theta)}k_{rot}\theta \tag{3}$$

Given a profile, this yields a force-deflection curve. This is however the inverse of the desired relationship. For a given F-D curve, a pulley profile should be calculated. To solve this issue, we set e.g. the following polynomial relation (from now on "radius equation"):

$$R(\theta) = b - a\theta \tag{4}$$

The displacement of the tendon can be calculated by taking a line integral (in polar form) on the pulley profile, as follows:

$$x(\theta) = \int_0^\theta \sqrt{r^2 + (\frac{dr}{d\theta})^2}d\theta \tag{5}$$

which, given the radius relation (Eq. 4), is further derived to:

$$x(\theta) = \int_0^\theta \sqrt{a^2 + b^2 + a^2\theta^2 - 2ab\theta}d\theta \tag{6}$$

This equation could be rewritten in terms of x, resulting in $\theta(x)$. This could be filled in into $F(\theta)$ (Eq. 3) which would result in $\tilde{F}(x)$. By altering its variables a, b, or changing $R(\theta)$ altogether, this formula could be equated with any desired F-D curve. However, rewriting Eq. 6 in terms of pulley angle is not trivial due to the nature of the equation.

This can be explained by drawing the system with bond graph theory, see Fig. 3, where *Sf* is the tendon velocity, and *MTF* the variable radius pulley. The modulated transformer forms a feedback loop, making it difficult to solve the system in the way presented above, since multiple solutions will be possible. This method heavily depends on the choice of radius equation, which decreases its flexibility. A certain choice of radius equation will likely limit the possible force-deflection solutions to a certain space. A change in desired curve could require recalculating the whole solution using different radius equations.

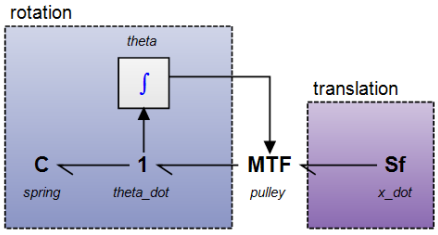

Fig. 3: Simple bond-graph representation of mechanism, 20-Sim

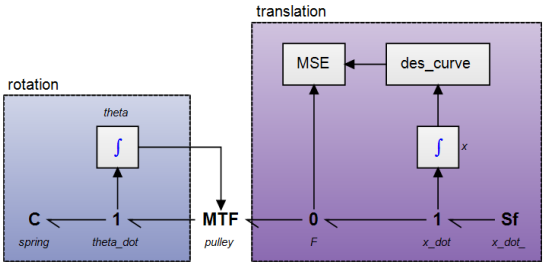

Fig. 4: Bond-graph of performance-metric approach, 20-Sim

D. Solve using Performance-metric

Due to the difficult nature of the symbolic approach, an optimization-based approach is looked at, using a performance metric to find an optimal solution. Using a similar bond-graph model as before (see Fig. 4), the Mean Squared Error (MSE) is calculated. Where *des_curve* is the desired force-deflection curve, and *MSE* the calculation of the error value. Integrating the resulting MSE value results in a performance metric of the current pulley profile parameters and spring constant value. The "multiple run" function in 20-Sim forms the optimization process. It sweeps a set of parameters (e.g. k_{rot}, a, b, from Eq. 4) within their respective bounds, and finds the combination that corresponds to the best performance metric (lowest integrated MSE). Three variable parameters result in multiple possible solutions, so one variable is constrained beforehand. Constraining more variables results in limited solutions. This should result in an optimal pulley profile following the selected radius equation (embedded in *MTF*). A more detailed continuation of this method is found in appendix A. In summary, this method is not sufficient for further use due to its dependency on the initial choice of radius equation.

E. Solve Iterative

The performance-metric approach severely constrains its application to a narrow range of desired force-deflection

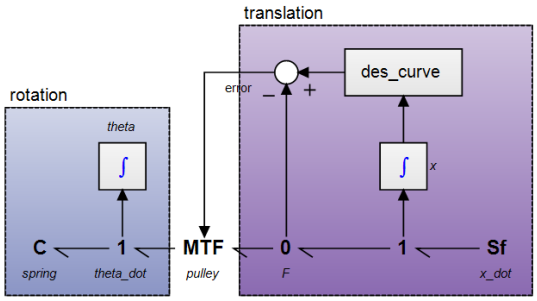

Fig. 5: Bond-graph of iterative approach, 20-Sim

curves. This is caused by the fact that a radius equation is set beforehand. Removing the need for such a predefined relation requires a major redesign. A numeric and iterative method could start of with a certain initial condition (e.g. initial pulley radius), and iterate on this radius such that the resulting F-D response converges to the desired force required at each deflection value. Such a method can be considered a feedback system. By adding an additional feedback loop to the bond-graph model of the NLS, this goal can be achieved. Given a certain deflection, an error can be produced between desired and measured force of the current design. Feeding back this error into the modulated transformer forms the loop (Fig. 5). By running this simulation for a certain time and tendon displacement velocity, a pulley profile can be generated that closely follows the desired NLS behaviour. By matching the simulation-time and displacement-velocity, we ensure the pulley supports the displacement range required. For all following simulations, a (realistic) torsion spring constant of $0.15\ \frac{Nm}{rad}$ is used.

The F-D curve used by Bluiminck [9] shows initial negative stiffness. Using this curve in the iterative method can cause problems, since negative stiffness is not realizable with the proposed mechanism. As previously mentioned, matching the specific curve shape is of no importance. Thus we construct a new approximate curve, similar to F_1. Note that we still take x in cm to make the parameters easier to read. Weaker F-D curve F_1 is chosen to limit tensile forces in the test setup. Substantial stresses can cause material deformation resulting in inconsistent results. We initially take the following approximate:

$$\tilde{F}_{approx_1} = ax^2 + bx \tag{7}$$

This ensures that a deflection of zero (x_0) will result in zero tensile force present. Parameter b shifts the initial radius since it determines what stiffness is present at x_0. b cannot equal to zero, since the initial profile radius will then diverge to infinity to eliminate any stiffness at x_0. a will shape the non-linearity of the F-D curve. For this use-case, $a = 1.6, b = 1.0$ are set and form the approximate desired F-D curve. From these initial parameters b is increased, sweeping various curves, shown in Fig. 7. The corresponding profiles are shown in Fig. 6. What can be observed is that a decrease in b results in higher initial radius. A sharp edge at the initial angle of the pulley is present, which is not desirable for manufacturing and operation. Note

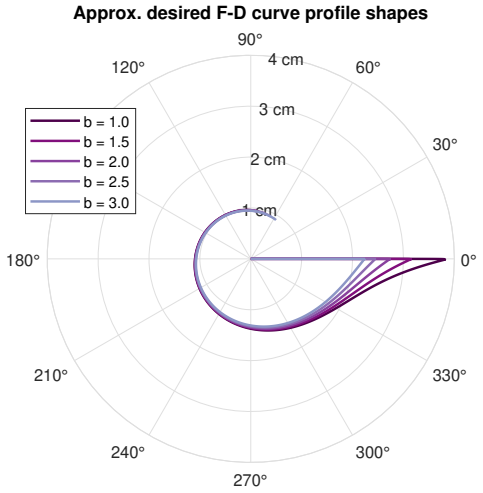

Fig. 6: Pulley shape from approx. F-D curve, sweeping b

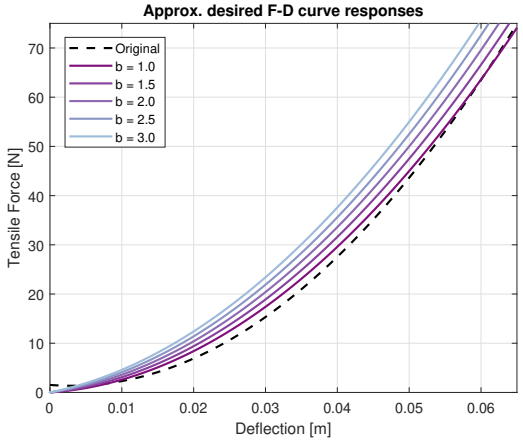

Fig. 7: Force-deflection from approx. F-D curve, sweeping b

the initially concave shape of the pulley, which is not allowed due to the approximations taken in Sec. II-B. An alternative curve approximation can be taken:

$$\tilde{F}_{appr_2} = ax^3 + bx \tag{8}$$

which, due to the higher order, is able to increase b further without losing non-linearity. For this use case $a = 0.2$ and $b = 2.5$ are chosen. The resulting pulley profile and F-D curve can be seen in Fig. 9, among others discussed in Sec. III-B. A lower a and higher b causes much faster increase in initial stiffness. No sharp edge nor convex shape is present anymore. With this result, this method can be concluded sufficient for further use. Note that the systems time to converge to desired curve is near instant, and removed from the profile data for manufacturing purposes. The simulation uses a proportional gain of 50, for fast convergence. Higher gain leads to an irregular profile surface due to unstable behaviour.

III. Design

Applying the theoretical approach on a realized NLS mechanism allows us to evaluate the method on real-world implementations. This section discusses both a realised implementation in a test-setup, the experiments to be carried out, and

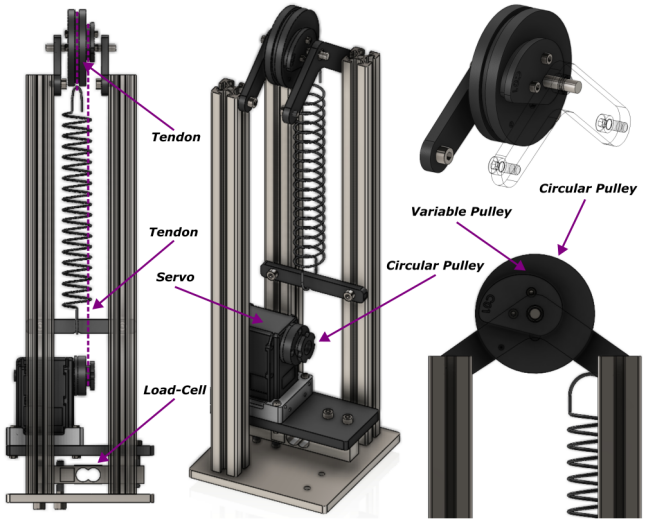

Fig. 8: Various views of the test-setup, SolidWorks

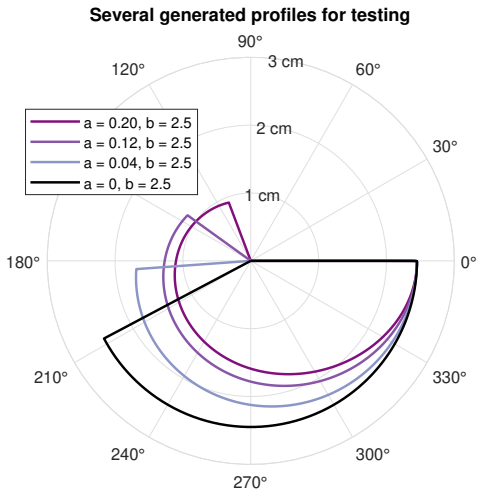

Fig. 9: Various generated pulley profiles for further measurements

a theoretical implementation of the mechanism in the gripper prototype.

A. Test-Setup design

Verifying F-D curves from generated profiles requires measurements of tensile force in and deflection of the tendon. Unlike in the gripper prototype, dynamically altering spring deflection directly with an extra actuator is not necessary. A spring between pulley profile and ground is sufficient. This static testing simplifies the test-setup. Fig. 8 shows the 3D-CAD model of the setup, along with clarifying annotations. Using the *MX-64AR* servo with a circular pulley, the tendon can be displaced. A *TAL220* load-cell with *HX711* amplifier measures the tensile force present within the tendon. The servo rests on a plastic platform that connects to a metal base via the load-cell/strain-gauge. Located in-line with the tendon, it measures the tensile force in said tendon. Pulley rotation data is acquired through the servo. Displacement of the tendon is derived from this data. A tendon connects the circular pulley to the variable pulley. A larger circular pulley with extension spring is placed on the axle of the variable pulley (Fig. 8). Due to the difficult installation of torsion springs an equivalent extension spring is used. The extension spring constant is $0.23\frac{N}{mm}$, which in combination with the circular pulley, is equivalent to a torsion spring constant of $0.15\frac{Nm}{rad}$. A second tendon connects circular pulley and spring. Note that finding springs with sufficient specifications (max. deflection, size, spring constant, etc.) can be difficult, as they are often either too large, or do not offer the range of tension required. The model shows a the fully extended state of the spring. An *Arduino Uno* with *Dynamixel Shield* controls the servo, and receives rotation and load-cell measurements. Fig. 1 shows the realized setup. A specific wire (*Spiderwire Dura 4 0.25mm*) is used that is resistant to stretching under load. A *MarkForged Mark II* printer with *Onyx CF Nylon* is used to fabricate all printed parts, preventing material bending and deformation as much as possible.

B. Experiments

Two experiments are carried out with the test-setup. As previously stated, the first experiment will verify generated profiles by measuring tensile force and deflection, resulting in F-D curves. Four different profiles are generated, with decreasing exponential factor a and constant b. This results in a profile shape going from the shape shown in Fig. 6 to a circular (linear spring behaviour) profile. This linear spring profile creates an opportunity to verify the system, without influence of several of the approximations taken. The array of profiles should show an incremental decrease in error between profiles originating from the tangent drift (Sec. II-B). Initial non-linear behaviour of the extension springs is circumvented by preloading the system at approximately $5N$.
The second experiment analyzes system hysteresis. Changes to behaviour depending on previous states (e.g. a switch of deflection direction) decreases consistency of the mechanism, which is undesired. Measuring both tensioning and loosening of the system provides a measure of hysteresis. The previous experiment is repeated, while also measuring the return to initial state. Lower servo RPM is used in this experiment to increase resolution, at the cost of more time spent in a high-stress environment.

C. Gripper Implementation

Following verification of the NLS unit, the mechanism should be integrated into the gripper prototype. This requires an altered configuration, due to the addition of an actuator that can dynamically change the torsion spring deflection. Due to time constraints this configuration has not been realized. A suggested implementation for integration is presented in Fig. 10. Limited space within the gripper requires minimizing space occupation. A force-sensor is no longer required. The extension spring is replaced with a torsion spring, lowering design size. This torsion spring directly connects to the pulley profile and servo axle. The axle holding the pulley is supported on two sides, to withstand the high forces from the tendon.

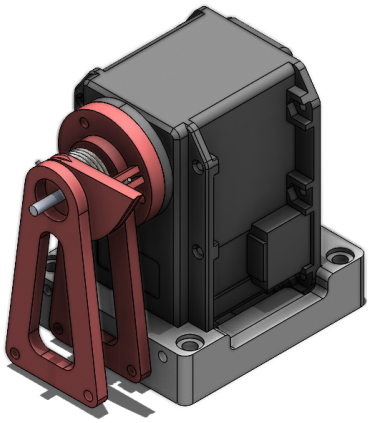

Fig. 10: Theoretical implementation of mechanism for gripper prototype, SolidWorks

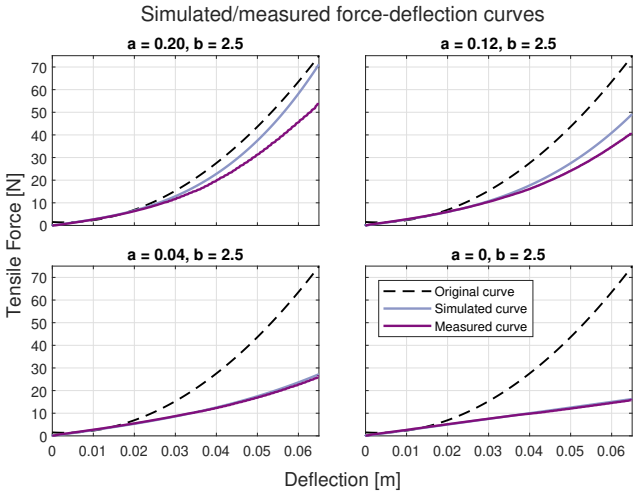

Fig. 11: Simulated and measured force-deflection curves

A pair of the presented NLS mechanisms forms an agonist-antagonist setup, and deflection of the torsion springs using the servos results in variable compliance and position control of the gripper phalanges. The footprint of this mechanism is approximately $20\text{x}10cm$, and approximately equal to the height of the servo. Size is drastically reduced compared to the currently implemented mechanism. Note that the spring model shown is not representative of any particular spring specification, as no torsion spring is used in the test-setup variant. *Dynamixel MX-64* servos are used within the gripper prototype and 3D-CAD model.

IV. Results

A. Force-Deflection Curves of Several Profiles

Force-Deflection measurements of an assortment of profiles are shown in Fig. 11. Each plot features the original F-D curve (F_1 [9]) for reference, followed by the simulated (desired) curve and its corresponding measured curve. The figure shows that increased F-D non-linearity corresponds to increased deviations between simulated and measured values. This corresponds to the expected results in Sec. II-B. The circular profile (bottom-right) closely follows desired behaviour. Finally, it should be noted that the preload on the system is not constant between experiments, and was manually tuned between every measurement.

B. Measured System Hysteresis

Results of the hysteresis experiment are shown in Fig. 12. Note that for both plots the (initial) bottom-side of the measured curves is the return to initial state and that this orientation switches at high deflection. At high deflection the linear response starts to deviate considerably from the simulation. This is also present in the previous linear curve measurement, but not clearly visible in the figure. Both profiles show a similar deviation between tensioning and loosening F-D curves. The worst-case displacement hysteresis measured on the linear and non-linear profiles is $0.17cm$ (2.6%) and $0.36cm$ (5.5% of total range) respectively. Deviation is less present toward higher deflection. The platform that connects servo to load-cell was observed to be slightly bending upwards while under high stresses for longer durations, suggesting material creep. Note that the hysteresis measurements were consistent across several experiments.

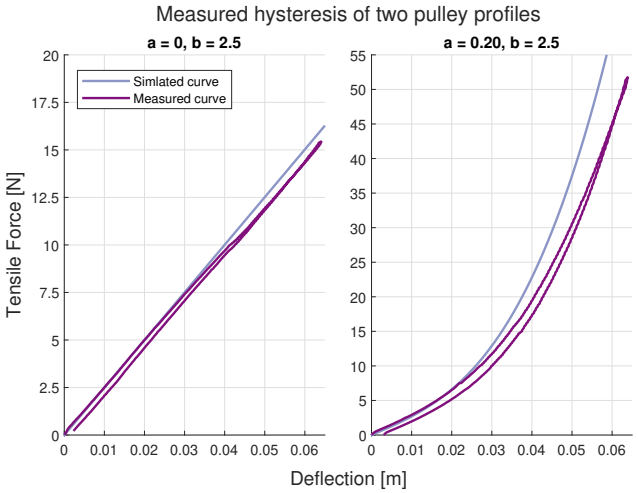

Fig. 12: Measured system hysteresis of two pulley profiles

V. Discussion

A. Force-Deflection Curves of Several Profiles

The measured force-deflection curves show a large deviation between simulations, especially higher non-linearity profiles. Close to zero deviation is present at the circular profile response. Thus, the main source of deviation is likely the tangent location approximate. However, other factors could have influenced the results. The $5N$ preload is not taken into account while generating profiles. Additionally, the specified $2.59N$ initial force requirement set by the spring manufacturer is not sufficient to eliminate all undesired initial behaviour of the system. This difference points to other non-idealities in the system, such as knot tightening. Moreover, the gradual

decrease in preload in between measurements suggests material creep of plastic parts, or loosening of knots. Flexing of the servo-base could result in a decrease in measured tensile force, since the load-cell setup requires rigid plates and joints for accurate measurements. Surface deformation is visible in areas where the tendon contacts 3D printed parts at a sharp angle. Note that irregular behaviour towards higher deflection, mostly apparent in the first plot, is caused by a lower load-cell sample-rate from a bug in the Arduino code.

B. Measured System Hysteresis

The main deviation between the tensioning and loosening phase (hysteresis) is likely a result of the non-idealities mentioned above. Loosening of tendons due to material creep or improper knots will lower the measured tensile force during the returning phase. The higher worst-case hysteresis of the non-linear profile is likely attributed to the higher forces present, thus causing more tendon loosening. The observed sudden deviation of the linear profile can be a result of material creep. The same behaviour is likely present in the non-linear profile measurement, but visually obstructed by the curve shape.
The rough surface finish of the several pulley "side-rails" showed signs of damaging the tendons, contributing to overall friction. This friction is likely a factor in causing the orientation switch of the tightening and loosening phases seen at higher deflection.

VI. Conclusion

In this paper, a design of a variable stiffness mechanism is presented, using a variable cam pulley and spring. A promising method to generate pulleys profiles to create non-linear springs is demonstrated. By using a feedback system, a pulley profile is generated that follows a desired force-deflection curve. Due to its iterative nature, realising a larger range of different desired curve is possible. Measurements on the test-setup show a promising realization of the concept, with measured profiles following intended force-deflection behaviour. Deviations between practical experiments and simulations can be attributed to both theoretical approximations like the tangent location shift, and practical non-idealities such as material creep and knot tightening. Accounting for the tangent location of the tendon on the pulley profile would likely improve performance. Additionally, a design suitable for gripper integration is presented. The low-friction nature of the mechanism, mechanical simplicity and minimized space occupation make the design a promising choice for future integration.

A. Future Work

Higher stiffness materials (e.g. machined aluminium or 3D-printed metals), and more effective ways to attach tendons to components could lead to more consistent measurements. Taking into account current approximations into the simulated model will increase the accuracy simulations, thus generate better performing profiles. The *20-sim* model can be more refined to reflect real-world operation by adding e.g. a tangent-solving system to the feedback loop. Considering the relative position of profile and servo is another aspect to be looked at.
Measurements to analyze hysteresis only measured a single deflection-cycle. Future experiments could increase the number of cycles, or vary the deflection speed, to allow for more extensive analysis on both creep and hysteresis of similar designs. Improving the quality of measured data with better sensors or improved serial logging could lead to more conclusive results.
Future implementations (possibly within the gripper prototype) could face difficulties acquiring torsion springs with sufficient parameters, since these might impose further constraints on the design and thus available profiles. To allow for a broader range of springs, a 3D helix-shape could be looked at, enabling usage of more than just 360° of pulley profile rotation. Additionally, this will increase the profile's length, allowing for increased deflection without sacrificing space occupation. Due to the small tendon diameter ($0.25mm$), a helix shape could be designed to be very flat. This might limit increased friction on the "side-rails" to a negligible level, keeping the low-friction nature of the mechanism as low as possible.

Acknowledgment

Firstly, I would like to thank my two supervisors, Dr. W. Roozing and Ir. B. Okken for their consistent guidance and support during the thesis. Secondly, the technicians at the RAM department of the University of Twente, A. Gąsienica and Q. Sablé for their assistance with the practical work related to the test setup.

References

[1] R. v. Ham, T. Sugar, B. Vanderborght, K. Hollander, and D. Lefeber, "Compliant actuator designs," *IEEE Robotics & Automation Magazine*, vol. 3, no. 16, pp. 81–94, 2009.
[2] S. A. Migliore, E. A. Brown, and S. P. DeWeerth, "Biologically inspired joint stiffness control," in *Proceedings of the 2005 IEEE international conference on robotics and automation*, pp. 4508–4513, IEEE, 2005.
[3] N. Schmit and M. Okada, "Synthesis of a non-circular cable spool to realize a nonlinear rotational spring," in *2011 IEEE/RSJ International Conference on Intelligent Robots and Systems*, pp. 762–767, IEEE, 2011.
[4] C. B. Yigit, E. Bayraktar, and P. Boyraz, "Low-cost variable stiffness joint design using translational variable radius pulleys," *Mechanism and Machine Theory*, vol. 130, pp. 203–219, 2018.
[5] J. Malzahn, E. Barrett, and N. Tsagarakis, "A rolling flexure mechanism for progressive stiffness actuators," in *2019 International Conference on Robotics and Automation (ICRA)*, pp. 8415–8421, 2019.
[6] D.-H. Kim and J.-H. Oh, "Hysteresis modeling for torque control of an elastomer series elastic actuator," *IEEE/ASME Transactions on Mechatronics*, vol. 24, no. 3, pp. 1316–1324, 2019.
[7] C. Jarrett and A. McDaid, "Modeling and feasibility of an elastomer-based series elastic actuator as a haptic interaction sensor for exoskeleton robotics," *IEEE/ASME Transactions on Mechatronics*, vol. 24, no. 3, pp. 1325–1333, 2019.
[8] B. Okken, S. Stramigioli, and W. Roozing, "Progressive series-elastic actuation with magnet-based non-linear elastic elements," in *2022 IEEE International Symposium on Safety, Security, and Rescue Robotics (SSRR)*, pp. 166–173, 2022.
[9] M. Bluiminck, "Modelling and control of underactuated finger-based gripper with adjustable compliance for grasping of varying and deformable objects," Master's thesis, University of Twente, 2022.

APPENDIX A
CONTINUATION OPTIMIZATION-BASED METHOD

Three different exemplary parameter sweeps are shown to discuss the quality of the result, and the limits of this method. The initial radius (b) is locked at 5cm, to ensure realistic pulley dimensions. Several different radius equations are used. The change in radius equation means parameter bounds are varied as well (to prevent simulation errors from number overflow). All sweep settings and corresponding results are listed in Tab. I.

TABLE I: Overview of three optimized sweeps

Sweep	$a \in$	b	$k_{rot} \in$	$R(\theta) =$	a	k_{rot}
1	$[1, 18]$e-3	0.05	$[0.1, 2.5]$	$b - a\theta$	0.015	1.912
2	$[1, 2.5]$e-3	0.05	$[0.1, 2.5]$	$b - a\sqrt{\theta}$	0.021	1.172
3	$[0.1, 12]$e-3	0.05	$[0.1, 3]$	$b - a\theta^2$	0.010	2.605

See resulting pulley shapes in Fig. 13, and F-D curves in Fig. 14. As shown in the figures, the optimized results do not overlap with the desired curve. A likely cause might be that the desired curve is not within the solution space of any of the presented radius equations. The equation required is most likely a rather complex and specific function, not easily found with an estimation. A change from $\sqrt{\theta}$ to θ^2 does not affect the resulting curve significantly. Note that the optimization function cannot sweep all parameters at once, nor over a large range. Many parameter combinations result in an error (likely numerical overflow) due to the Backward Differentiation Formula used by 20-Sim. This method, utilizing a parameter sweep to find the optimal result, is not deemed sufficient for further use. Any change in desired curve requires finding a different suitable radius equation, if one can be found at all.

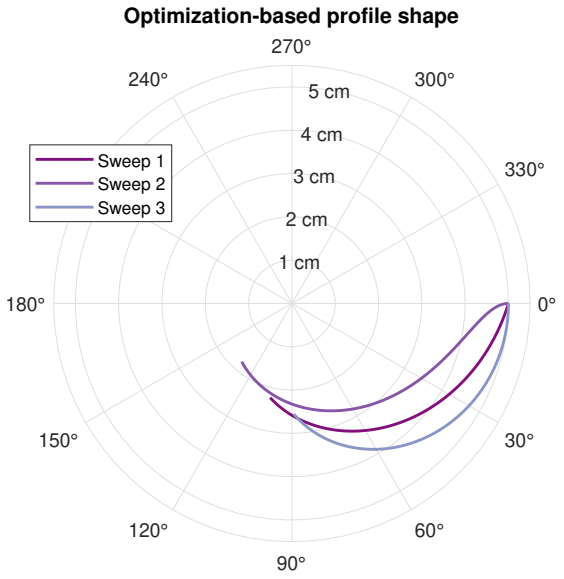

Fig. 13: Optimized pulley shape result

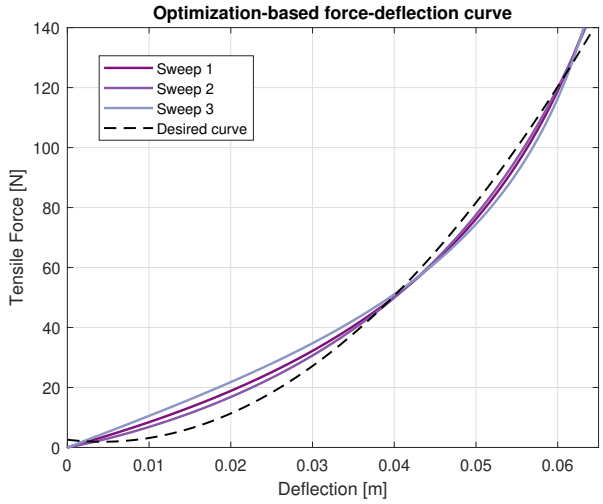

Fig. 14: Optimized force-deflection curve result